Nuclear Engineering and Technology 50 (2018) 860–868

Contents lists available at ScienceDirect

Nuclear Engineering and Technology

journal homepage: www.elsevier.com/locate/net

Original Article

Development of earthquake instrumentation for shutdown and restart criteria of the nuclear power plant using multivariable decision-making process

Md M. Hasan, Joyce K. Mayaka, Jae C. Jung*

Department of Nuclear Power Plant Engineering, KEPCO International Nuclear Graduate School (KINGS), 658-91 Haemajj-ro, Seosaeng-myeon, Ulju-gun, Ulsan 689-882, Republic of Korea

ARTICLE INFO

Article history:
Received 29 December 2017
Received in revised form
20 March 2018
Accepted 3 April 2018
Available online 10 April 2018

Keywords:
Fatigue
Operating Basis Earthquake
Peak Ground Acceleration
Safe Shutdown Earthquake
Structure, System, and Components

ABSTRACT

This article presents a new design of earthquake instrumentation that is suitable for quick decision-making after the seismic event at the nuclear power plant (NPP). The main objective of this work is to ensure more availability of the NPP by expediting walk-down period when the seismic wave is incident. In general, the decision-making to restart the NPP after the seismic event requires more than 1 month if an earthquake exceeds operating basis earthquake level. It affects to the plant availability significantly. Unnecessary shutdown can be skipped through quick assessments of operating basis earthquake, safe shutdown earthquake events, and damage status to structure, system, and components. Multidecision parameters such as cumulative absolute velocity, peak ground acceleration, Modified Mercalli Intensity Scale, floor response spectrum, and cumulative fatigue are discussed. The implementation scope on the field-programmable gate array platform of this work is limited to cumulative absolute velocity, peak ground acceleration, and Modified Mercalli Intensity. It can ensure better availability of the plant through integrated decision-making process by automatic assessment of NPP structure, system, and components.

1. Introduction

Many nuclear power plants (NPPs) in the world face unnecessary shutdown and wastage time to follow long procedures to restart the plant. Onagawa Plant, Japan, 2005—Base mat accelerations exceeded safe shutdown earthquake (SSE) ground motion. No damage was found to safety-related (SR) structure, system, and components (SSCs). Time to restart was 5–7 months for three units [1]. Shika Plant, Japan, 2007—In-structure response spectra (ISRS) exceeded SSE-based ISRS. No damage was observed to SR SSCs. Time to restart was 1 year [1]. Kashiwazaki-Kariwa Plant, Japan, 2007—All ground spectra exceeded SSE; ISRS significantly exceeded ISRS for SSE. No damage was found in SR SSCs. Time to restart was 22–40 months for seven units [1]. North Anna Plant, VA, USA, 2011—Base mat spectra exceeded SSE above and below 10 Hz. No damage was detected to SR SSCs. Time to restart was 2–3 months for two units (information provided by Dominion Energy). On the 12th of September 2016, South Korea experienced the most powerful earthquake ever recorded in the country since measurements began in 1978. A 5.8-magnitude earthquake struck the historic city of Gyeongju, and the people have been subject to a series of aftershocks affecting their daily lives [2]. However, the frequency of the earthquake wave was higher than 16 Hz, and a disastrous falling down of structure was not experienced. Continuous research is being carried out for accurate response to an earthquake event to avoid pseudo shutdown of the plant. Calculation of cumulative absolute velocity (CAV) has been revised as standardized cumulative absolute velocity [3]. But, a well-defined complete response to an earthquake event is still necessary for more availability of the plant with confirming integrity of SSC. Therefore, existing earthquake instrumentation and procedures should be reviewed and updated.

Design of earthquake instrumentation which is composed of Micro-Electro-Mechanical System (MEMS) sensor and field-programmable gate array (FPGA)–based seismic data processing system is developed in this work for quick assessment of the events comparing with design operating basis earthquake (OBE) and SSE levels of the plants. In addition, this design suggests a method to assess fatigue levels of NPP SSCs. Seismic sensor and its data

* *Corresponding author.*
E-mail addresses: mehediapece@yahoo.com (M.M. Hasan), joicmayaka@gmail.com (J.K. Mayaka), jcjung@kings.ac.kr (J.C. Jung).

https://doi.org/10.1016/j.net.2018.04.004

processing are the major parts of the earthquake instrumentation. The traditional sensor performs tremendous job in earthquake instrumentation, but it suffers significant reduction in recorded velocity-domain amplitudes and below their natural frequency. MEMS sensor, which is applied to our design, has multidimensional advantage over traditional sensors. The Digital Sensor Unit (DSU) consumes low power and shows accurate functionality at any tilt angle. It is reliable for all operations with high performance and power efficiency. The data from a single ground location is digitized by the DSU. It records accurately the ground motion on all the three axes allowed by its three orthogonal components. On the other hand, the analog sensor records the vertical component only. The performance parameters such as noise floor, full scale, dynamic range, sensitivity, and data quality prove suitability of the MEMS sensor over the traditional geophone sensor [4–6]. An important factor is that the installation and maintenance cost of the MEMS is lower than that of other sensors. MEMS response to acceleration is constant from frequency 0 Hz to 800 Hz, both in amplitude and in phase, which is optimal to capture a broadband signal [7]. Therefore, MEMS sensor response is linear in the acceleration domain down to direct current, and there should be no attenuation and sufficient signal-to-noise ratio toward the low end of the spectrum. The MEMS sensor shows the best potentiality among various seismic sensors for digital data output which is essential for interfacing with FPGA. This accelerates to design MEMS-based earthquake instrumentation with FPGA data processing system for NPPs.

After designing the new earthquake instrumentation, the various earthquake-level parameters are clarified as mathematical equation and theoretical explanation for synthesizing the design. It can provide automatic information on various parameters. If CAV exceeds threshold level (0.16 g s), OBE level exceeds. The exceedance of SSE level can be confirmed by comparing receiving and design FRS. Receiving FRS is the calculated FRS found from recorded earthquake event. If it exceeds design FRS, then the impact of the earthquake exceeds SSE level. The system can also give peak ground acceleration (PGA), Modified Mercalli Intensity (MMI), and cumulative fatigue information. Fatigue can provide current damage status information of the equipment and structure of the plant. However, in this study, CAV, PGA, and MMI parameters are focused for implementation of the FPGA platform. FRS and cumulative fatigue are excluded in consideration of workload of this study. This study will help to do quick assessment of the earthquake events and encourage updating the existing procedure in response to an earthquake event so that more availability of the plant can be ensured.

2. Materials and methods

2.1. Design architecture

Earthquake instrumentation consisting of the DSU and FPGA-based data processing system for the NPP is newly designed. The design consists of two blocks. One is for MEMS digital sensor, and another block is FPGA board. There is a relationship among magnitude, wave frequency, and the devastating power of earthquake. Seismic-measuring and detection instrumentation, i.e., sensor has been improved to detect the frequency and magnitude of the earthquake wave effectively. A single seismic instrument can be defined as mass, spring, and dashpot as shown in Fig. 1 through investigating both theory and application of earthquake instruments [8]. Seismic energy is absorbed by the dashpot. This spring-mass-dashpot system can be expressed using Newton's second law as represented in Equation (1).

$$\text{D.E.)}\ m\ddot{y} = -ky - b\dot{y} + u \tag{1}$$

$$\text{T.F.)}\ ms^2Y(s) = -kY(s) - bsY(s) + U(s) \tag{2}$$

$$G(s) = \frac{Y(s)}{U(s)} = \frac{1}{ms^2 + bs + k} \tag{3}$$

The mathematical expression of the system aforementioned can be expressed as Equation (1). The transfer function of Equation (1) can be obtained as Equations (2) and (3) by taking Laplace transformation. The motion of the mass as a function of the ground displacement is expressed by a differential equation resulting from the equilibrium of forces as shown in Equation (4) [9].

$$F_s + F_r + F_g = 0[9] \tag{4}$$

where $F_s = -kx$ (F_s is force due to spring constant, s refers to spring, k is spring constant, and x is mass displacement).

$F_r = -b\dot{x}$ (F_r is force due to friction, r refers to friction, and b is friction coefficient).
$F_g = -m\ddot{u}$ (F_g is force due to ground acceleration, g refers to ground, m is spring mass, and u is the ground displacement).

The digital sensor which follows same rules which contains inertial mass, analog-to-digital converter, feedback, force-feedback actuator, and digital filter is shown in Fig. 2. In the digital sensor, a MEMS casing (blue) is attached to a sensor casing (not represented). Stiff springs (black) maintain the inertial mass (green) which moves with casing/ground motions. Electrodes (red) measure the displacements of the inertial mass, when it is subjected to seismic acceleration. A closed-loop MEMS accelerometer is driven mainly by the electrostatic feedback force; so, sensitivity is no longer a function of such mechanical parameters. The closed loop also minimizes the mass displacement because any force on the mass induced by acceleration is counteracted immediately by an opposite electrostatic force. A force-feedback actuator generates within microseconds a voltage that brings the electrodes back to their rest positions. Actually, the original mass displacement is very small, and it is negligible (a few nanometers), and spring-stiffness nonlinearity does not induce any distortion. The FPGA board receives ground motion acceleration data from the digital filter of the sensor and performs interfacing with the sensor. Here, seismic signal analysis is analyzed for calculating CAV, MMI, PGA, FRS, and cumulative fatigue. It gives OBE, SSE-level vulnerability alarm, and SSC damage information to the status logging and external interface.

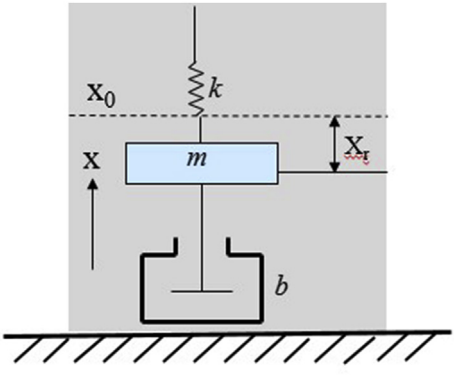

Fig. 1. Spring-mass-dashpot system.

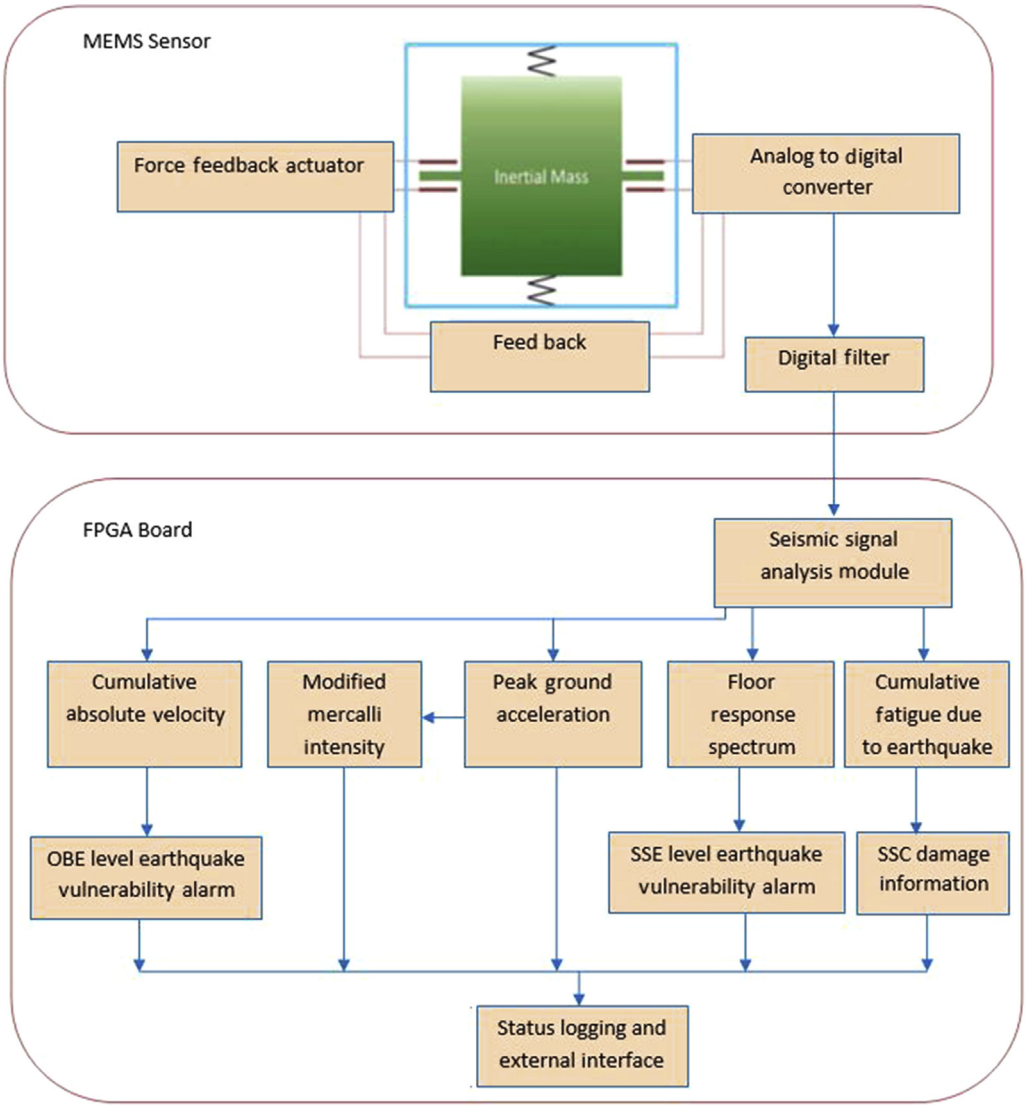

Fig. 2. Schematic of earthquake instrumentation which combines SSC vulnerability and integrity decision after seismic incident.
SSC, structure, system, and component.

2.2. Design synthesis

2.2.1. CAV criteria

The CAV value indicates whether the earthquake exceeds the OBE level or not. If it reaches a threshold value, the event is considered as exceeding OBE level. The CAV was originally defined as Equation (5) [3].

$$CAV = \int_{0}^{t_{max}} |a(t)|dt \tag{5}$$

where a(t) = acceleration time history, t_{max} = duration of record.

The threshold value was 0.30 g s. To avoid low nondamaging acceleration, CAV is standardized as Equation (6) [3].

$$CAV_{Total} = CAV_i + \int_{t_{i-1}}^{i} |a(t)|dt \tag{6}$$

where a(t) = acceleration values in a one-second interval where at least one value exceeds 0.025 g, i = 1, and n equal to the record length in seconds. The revised CAV threshold is 0.16 g s.

2.2.2. Peak ground acceleration

The maximum ground acceleration measured during earthquake vibration at a site is defined as PGA. Generally, earthquake vibration occurs in all the three directions. The PGA can be divided into vertical and horizon components. Normally, the components in the vertical direction are smaller than those in the horizontal direction. But, it is not true for all times, especially close to massive earthquake. In earthquake engineering, PGA is a significant criterion. It is also known as intensity measure. PGA is mathematically expressed as Equation (7) [10].

$$PGA = Max\{|a(t)|\} \tag{7}$$

where a(t) = acceleration value at time t.

2.2.3. MMI scale

Intensity can be defined as effect of an earthquake event on the Earth's surface. The intensity scale is formed of a series of certain

key responses such as total destruction, damage to chimneys, movement of furniture, and minimum people awakening. For evaluating the effects of earthquake, different intensity scales have been developed across the last several hundred years. MMI is the currently used scale in the United States. American seismologists Harry Wood and Frank Neumann developed this scale in 1931. This scale is designed with Roman numerals and is composed of increasing levels of intensity that range from indiscernible shaking to calamitous destruction. It is not designed by mathematical relation. It is a capricious ranking based on observed effects. Table 1 shows relationship between MMI and PGA [11]. MMI VI is conservatively identified as exceeding the OBE. Threshold of earthquake damage is greater than VI i.e., equal to VII. However, damage to building of good design and construction does not occur until MMI VIII [10].

2.2.4. Design SSE FRS exceedance criteria

FRS are used for design SSE exceedance criteria. One vertical and two horizontal response spectra can be determined from the time-history motions of the supporting structure at the various equipment-support locations and floors of interest. It is important that the spectrum ordinates be computed at the natural frequencies of the supporting structure and at frequencies sufficiently close to produce accurate response spectra. Spectrum peaks normally would be anticipated to occur at the natural frequencies of the supporting structure. Suggested frequency intervals for calculation of response spectra are given in Table 2 [12].

In long-term evaluation to calculate seismic load, FRS is needed. Generation of FRS is the example of calculation of seismic load. Floor response spectra should be generated for all elevations of interest based on the actual earthquake ground motion records using realistic, median-centered methods (e.g., best estimate modeling and damping). The calculated FRS based on the actual earthquake record should be compared with the SSE FRS. If the calculated FRS for any floor elevation are enveloped by the SSE FRS (i.e., are less than the SSE FRS at all frequencies of interest), then the design basis for floor-mounted equipment and piping on that floor has not been exceeded, and seismic reevaluation of equipment and piping on that floor is not required. However, if the calculated FRS for any floor elevation exceeds the SSE FRS at any frequency, then the design basis for floor-mounted equipment and piping, as well as the structure itself, may have been exceeded, and further evaluation should be performed [13]. Three sets of time-history acceleration data are considered as the first set data are exact g value data. Second set and third set data are taken as 50% and 20% of exact g value data, respectively. For getting response spectrum, automatic spectrum tool PRISM is used. Fig. 3 shows elastic response spectra and Fig. 4 shows constant ductility inelastic response spectra for three sets of time-history acceleration data and comparison with floor design response spectra of Kori 1 Auxiliary building. Analyzing the above spectrum, it is observed that response spectrum for exact g value data exceeds design FRS at some frequencies for both elastic and inelastic structure. In addition to the elastic structure, the response spectrum for 50% g value exceeds SSE design FRS. The other cases of the response spectrum are enveloped by the design FRS.

Table 1
Relationship between MMI and PGA.

Intensity	Peak ground acceleration (g)
I	<0.0017
II–III	0.0017–0.014
IV	0.014–0.039
V	0.039–0.092
VI	0.092–0.18
VII	0.18–0.34
VIII	0.34–0.65
IX	0.65–1.24
X+	>1.24

MMI, Modified Mercalli Intensity; PGA, Peak ground acceleration.

Table 2
Suggested frequency intervals.

Frequency range (Hz)	Increment (Hz)
0.2–3.0	0.10
3.0–3.6	0.15
3.6–5.0	0.20
5.0–8.0	0.25
8.0–15.0	0.50
15.0–18.0	1.0
18.0–22.0	2.0
22.0–34.0	3.0

2.2.5. Fatigue and cumulative fatigue estimation and stability of SSC

One of the SSCs that are expected to be most affected by fatigue is piping that operates in high-temperature and high-pressure environments, such as NPPs. When a seismic wave is introduced into this pipe, cracks are formed by continuous fatigue phenomenon. If a numerical analysis model capable of continuously detecting such phenomena is used, an alarm can be generated above the pipe fatigue limit [14]. Even if the seismic wave is of such a low magnitude that it does not cause instantaneous destruction fatigue, its cumulative cyclic loading can increase the probability of fatigue cracks in the pipe, especially in the bend section. These fatigue cracks can be predicted by numerical analysis. Numerical analysis predicts the time of crack formation when displacement is applied to the pipe and performs analysis on displacements of various sizes. Because the relationship between the size of the displacement and the time of the crack formation according to the shape and properties of the bend of piping can be grasped, it is used as a database.

In the case of structures such as bridges, the fatigue damage due to each fatigue load is obtained by using the S–N curve based on the estimation of the stiffness, and the remaining life is evaluated by the cumulative damage method. The S–N curve is the frequency of the seismic waves and the range of stress. The unit of stress is MPa. The cumulative damage of concrete structures such as bridges is estimated to be fatigue failure if the cumulative contribution of fatigue due to load components at different periods is combined. The fatigue damage degree, d_i, due to stress σ is expressed as Equation (8) [15].

$$d_i = \frac{n_i(\sigma)}{N_i(\sigma)} \tag{8}$$

where n_i is the number of times the stress σ occurs due to seismic wave and N_i is the number of times the fatigue failure occurs due to this stress σ. The total fatigue damage, that is D, can be calculated by algebraically summing the fatigue failure diagrams generated by the structures with different K loads over the unit time. The Equation (9) gives the assumption that fatigue failure occurs when total fatigue damage is greater than η, where T is the fatigue life [15].

$$D = \sum_{i=1}^{T}\sum_{j=1}^{K} d_{ij} = \sum_{i=1}^{T}\sum_{j=1}^{K} \frac{n_{ij}(\sigma)}{N_{ij}(\sigma)} \geq \eta \tag{9}$$

2.3. Evaluation of the system using enhanced functional flow block diagram

Complexity and execution time of existing earthquake instrumentation and our newly designed system are evaluated through functional analysis using enhanced functional flow block diagram (EFFBD). The EFFBD of the existing system is shown in Fig. 5.

Core-9 simulation and execution time of geophone-based existing earthquake instrumentation are shown in Fig. 6. Simulated diagram shows the time consumed by each function. In Fig. 6, the total execution time is 62.37 units. Time consumption by each function is calculated by software itself automatically when it is run. Exact time units are not mentioned in the software. It actually shows the comparative spent time of each function.

The EFFBD of newly designed earthquake instrumentation with FPGA data processing system is shown in Fig. 7.

Core-9 simulation and execution time of the newly designed Earthquake Instrumentation with FPGA data processing system are shown in Fig. 8.

From aforementioned enhanced functional flow diagrams and core-9 simulation, it is observed that the new system has easier data accessibility and ensures integrated decision-making process. The execution time of the newly designed earthquake instrumentation with FPGA data processing system is comparatively low (57.37 units), whereas the existing earthquake instrumentation is 62.37 units. Therefore, with low execution time and easy accessibility to multidecision parameters (CAV, PGA, MMI, FRS, and cumulative fatigue), the modified system can give quick

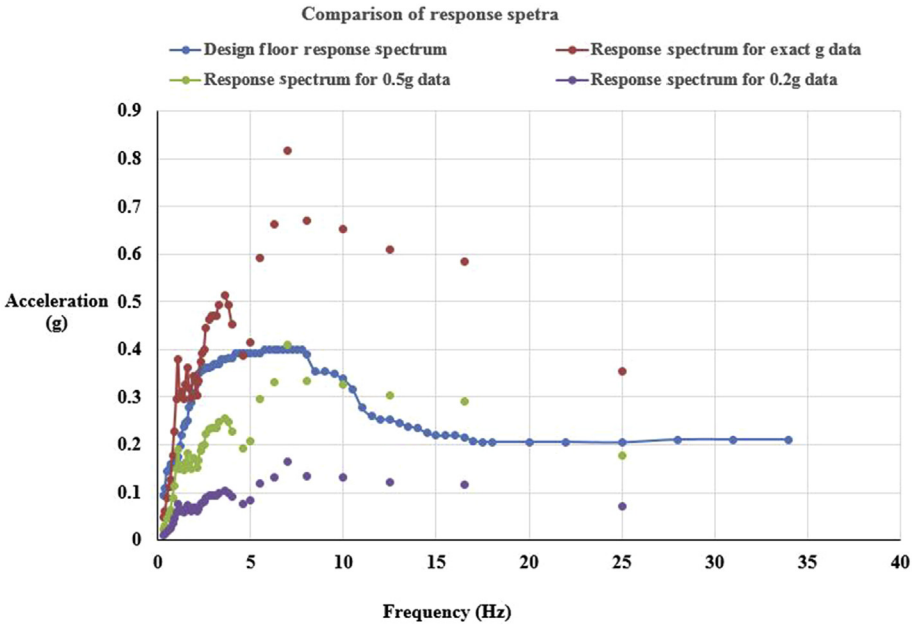

Fig. 3. Comparison of response spectrum considering elastic spectra structure.

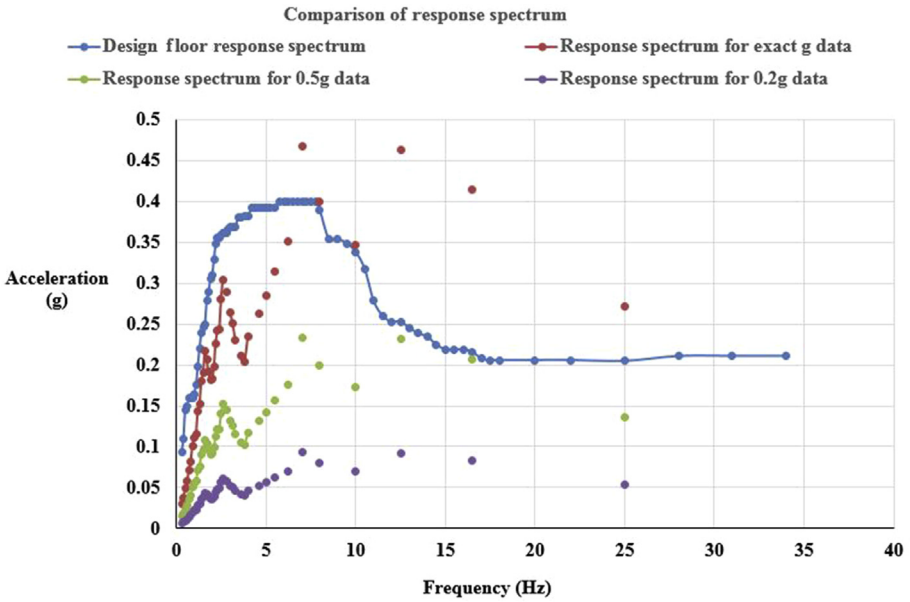

Fig. 4. Comparison of response spectrum considering constant ductility inelastic structure.

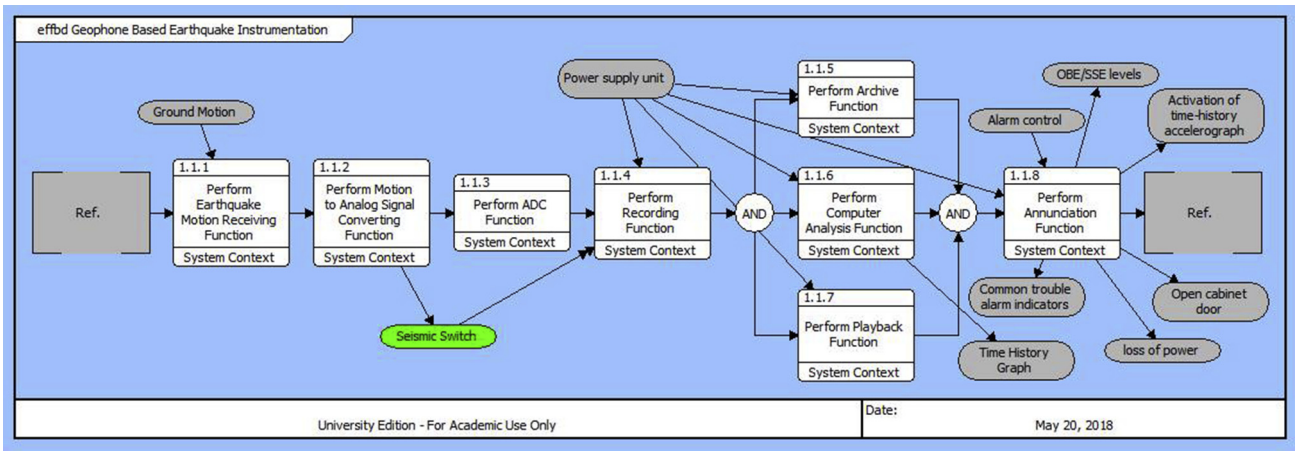

Fig. 5. EFFBD of the existing earthquake instrumentation.
EFFBD, enhanced functional flow block diagram.

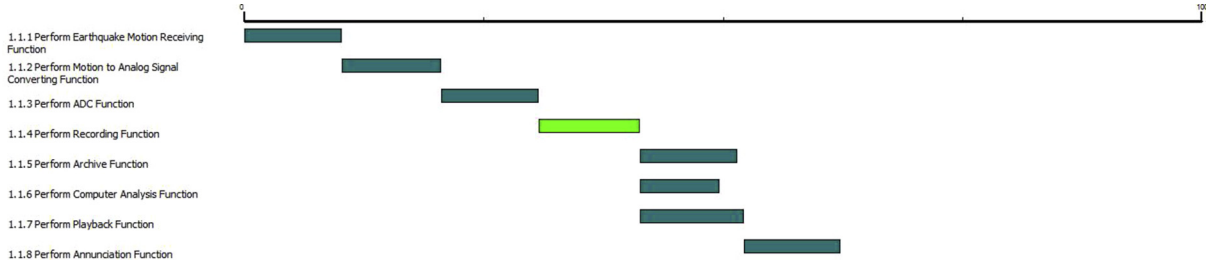

Fig. 6. Core-9 simulation of geophone-based existing earthquake instrumentation.

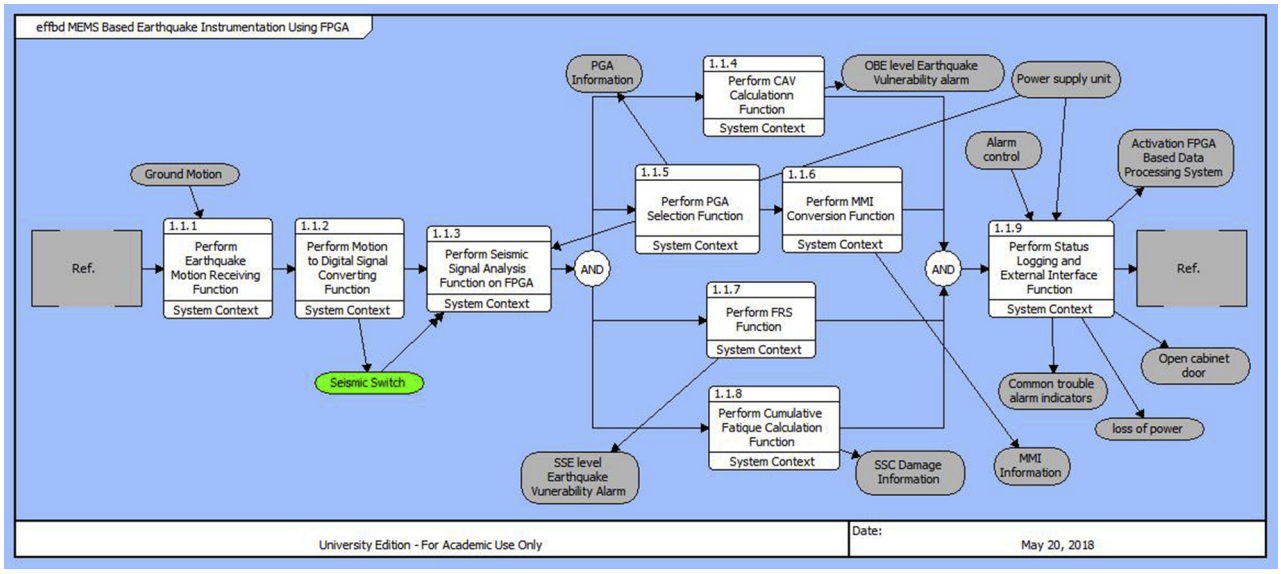

Fig. 7. EFFBD of MEMS-based earthquake instrumentation with FPGA data processing system.
EFFBD, enhanced functional flow block diagram; FPGA, field-programmable gate array; MEMS, Micro-Electro-Mechanical System.

and authentic parameter information to evaluate earthquake events.

2.4. Implementation on FPGA and test results

Seismic data processing system is implemented through VHSIC Hardware Description Language (VHDL) coding using Xilinx Vivado program. Implementation is performed on the FPGA platform. Implementation scope is limited as considering only three parameters, i.e., CAV, PGA, and MMI, excluding FRS and fatigue from the design for reducing workload of this work. Fukushima Station Code FKS003 data on 11 March, 2011, downloaded from the Strong Motion Center website are used (Direction E-W) [16]. Thousand data around PGA value are picked where the sample rate is 100 samples/s, i.e., the total time is 10 seconds. We consider here three cases—Case 1: 20% of exact g value data, Case 2: 50% of exact g value

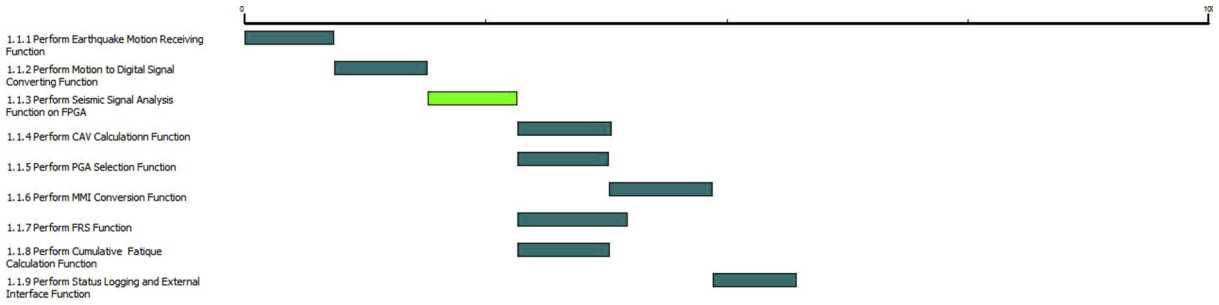

Fig. 8. Core-9 simulation of the new earthquake instrumentation with FPGA data processing system.
FPGA, field-programmable gate array.

data, and Case 3: Exact g value data. Table 3 shows expected results from FPGA board. Before implementation, we get possible results using Microsoft Excel program as shown in Table 4.

Fig. 9 shows outputs results and status for case 3 on the FPGA board after programming.

Verifying the results with FPGA outputs as shown in Table 5, it is observed that the two outputs are almost same with negligible differences.

3. Results and discussion

The purpose of the seismic monitoring system is to detect, record, and indicate earthquake-induced motion at various locations in and around the NPP so that operators can take necessary measures to protect personnel, plant components, and the environment from radioactive release or shut down the NPP safely, if required. In the existing earthquake instrumentation, the seismic sensors are installed at free-field, containment structure (one at the foundation and two at the higher elevation), and independent seismic category I structure (one at the foundation and one at a higher elevation) [17]. According to the existing earthquake response procedure, when earthquake is felt, the operator has to take immediate actions such as walk-down inspection and evaluation of ground motion records whether the plant tripped or not [18]. If OBE level is exceeded, the plant needs to be shut down. Afterward, further inspection and test have to be performed which is time-consuming. Normally, it takes 1 month to several months. The new conceptual design contains MEMS digital sensor. Because of low weight, the digital sensor can be installed beside the various locations of the NPP, such as safety classes 1, 2, and 3, as well as nonnuclear safety equipment. Multidecision parameters of the new design such as CAV can give OBE exceedance information, FRS can give design SSE exceedance information, and cumulative fatigue can give SSCs damage status of the NPP. Recent experience has demonstrated the need for guidance to nuclear plant owners and operators on the appropriate response to earthquake, particularly the more frequent, low-level earthquake which are clearly felt and/or measured at the site, but which have little or no potential for damage. If the earthquake level exceeds OBE level observing CAV, PGA, and MMI, the new data processing system can avoid expanded inspections which frequently decrease the plant availability. Because cumulative fatigue information not only depends on the last earthquake events but also considers the previous earthquake level and its impacts on the SSCs, it can reduce operator walk-down inspections load. The response to an earthquake of the present system and new design system is shown as flow diagram in Fig. 10.

Table 3
Expected outputs status from FPGA for the three cases.

Case	OBE exceedance criteria CAV level, threshold values (0.16 g s)	PGA indication (g)	MMI indication
1	Not exceed	PGA information	MMI information
2	Exceed	PGA information	MMI information
3	Exceed	PGA information	MMI information

CAV, cumulative absolute velocity; MMI, Modified Mercalli Intensity; OBE, operating basis earthquake; PGA, peak ground acceleration.

Table 4
Outputs results from MS excel sheet for the three cases.

Case	OBE exceedance criteria CAV level, threshold values (0.16 g s)	PGA (g)	MMI scale
1	Not exceed (0.141141)	0.064262	V
2	Exceed (0.352853)	0.160654	VI
3	Exceed (0.70570514)	0.321308	VII

CAV, cumulative absolute velocity; MMI, Modified Mercalli Intensity; PGA, peak ground acceleration.

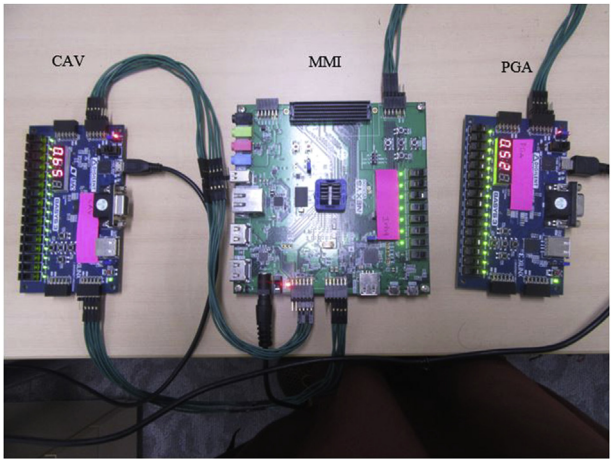

Fig. 9. FPGA board after programming.
FPGA, field-programmable gate array.

Table 5
Outputs results from FPGA for the three cases.

Case	OBE exceedance criteria CAV level, threshold values (0.16 g s)		PGA indication (g)		MMI scale
	Hexadecimal	Decimal	Hexadecimal	Decimal	No. of LED ON
1	0.24	0.140625	0.10	0.0625	V
2	0.5A	0.3515625	0.29	0.16015625	VI
3	0.b5	0.70703125	0.52	0.3203125	VII

CAV, cumulative absolute velocity; FPGA, field-programmable gate array; PGA, peak ground acceleration.

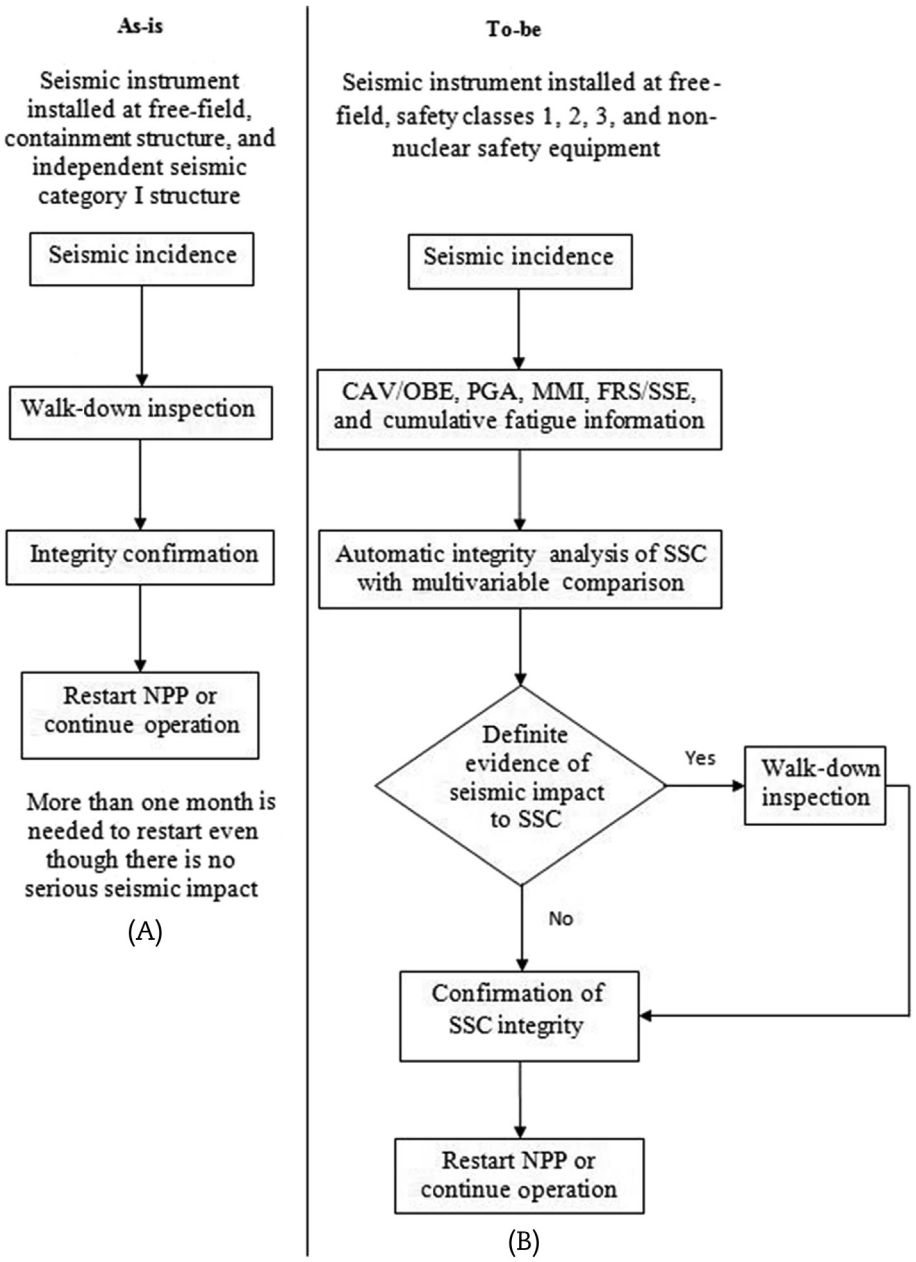

Fig. 10. Response to an earthquake. (A) Present earthquake response. (B) Earthquake response for the new design.
CAV, cumulative absolute velocity; FRS, floor response spectrum; MMI, Modified Mercalli Intensity; OBE, operating basis earthquake; NPP, nuclear power plant; PGA, peak ground acceleration; SSE, shutdown earthquake event.

However, we limited our implementation only for three parameters, i.e., CAV, PGA, and MMI at this stage for reducing workload. Verifying outputs from FPGA with MS Excel sheet, it is observed that the results are almost same with little differences. It proves the applicability of FPGA in seismic data–processing system.

Ground motion information recorded from various locations of the plant will be evaluated promptly after an earthquake as OBE level, SSE level, and SSC damage status which can help to follow response procedures quickly with more clarity. The quality of any developed system can be measured and evaluated through Measurements of Effectiveness (MOEs) and Measurements of Performance (MOPs). MOEs determine and elucidate system effectiveness that contemplates inclusive customer supposition and satisfaction. It is related to execute the customer's aim. Key MOEs include reliability, operability, safety, mission performance, etc. MOP measures attributes considered as important to ensure that the system has the capability to achieve operational objectives. MOP is applied to evaluate whether the system satisfy design or performance requirements that are obligatory to satisfy MOE. MOE and MOP of the new system are given in Table 6.

Table 6
MOE and MOP of the new system.

MOE	Low instrumentation cost, availability of the plant, and maintainability
MOP	Reduce human workload after the seismic incidence (for walk-down process), automated decision-making process for SSC integrity and fatigue, and easy data accessibility

The new earthquake instrumentation is conceptually designed with FPGA-based seismic data analysis system. The design is evaluated and compared by constructing EFFBD of the existing earthquake instrumentation and new earthquake instrumentation design. We get comparatively low execution time (57.37 units) than the present instrumentation (62.37 units). The applicability of FPGA for seismic data processing is proved by implementation of three parameters (CAV, PGA, and MMI) of the design. The output results found from the FPGA platform are almost same with the results calculated from MS Excel sheet.

The absence of clear, detailed, and graded procedures for nuclear plant response to an earthquake may result in not only unnecessary shutdown but also unnecessary inspections, tests, and analyses of plant SSCs and make extensive delays in plant restart. The new system has low instrumentation cost. It is easily maintainable. It reduces human workload after earthquake events. It can quickly assess the earthquake levels. Therefore, MOE and MOP are enhanced by doing this work. With low execution time, it can ensure better availability of the plant through integrated decision-making process by automatic assessment of NPP SSCs. Design SSE FRS exceedance criteria and cumulative fatigue due to earthquake, establishing clear relationship between earthquake acceleration and corresponding fatigue levels of SSC, can be implemented on the FPGA platform in future.

Conflict of interest

There is no conflict of interest.

Acknowledgments

This work was supported by the 2017 Research fund of the KEPCO International Nuclear Graduate School (KINGS), Republic of Korea.

References

[1] IAEA, Earthquake Preparedness and Response for Nuclear Power Plants, International Atomic Energy Agency, Viena, 2011. Safety Report Series No. 66.
[2] Strongest-everearthquake Hits Korea, Tremors Felt Nationwide, The Korea Times, September 12, 2016 [Online]. [Accessed 10 2016].
[3] EPRI, Standardization of the Cumulative Absolute Velocity, Yankee Atomic Electric Company, 1991. EPRI TR-100082.
[4] N. Tellier, J. Lainé, Understanding MEMS-based digital seismic sensors, First Break 35 (January 2017) 93–100.
[5] M. Moreau, J. Lainé, M. Serrut, MEMS-based accelerometers - the quest for low frequencies and weak signals, in: We P04 06, 76th EAGE Conference & Exhibition, Amsterdam RAI, The Netherlands, June 2014, pp. 16–19.
[6] J. Lainé, D. Mougenot, A High-sensitivity MEMS-based Accelerometer, The Leading Edge, November 2014, pp. 1234–1242.
[7] D. Mougenot, N. Thorburn, MEMS-based 3C accelerometers for land seismic acquisition: is it time? Leading Edge 23 (3) (2004) 246–250. http://www.sercel.com/products/Lists/ProductPublication/Sercel-MEMS-based-3C-accelerometers-for-land-seismic-acquisition-1.pdf.
[8] K. Ogata, Modern Control Engineering, third ed., Prentice-Hal, New Jersey, 1997, pp. 83–84. Chapter 3.
[9] J.C. Jung, Earthquake Instrumentation, Earthquakes - Tectonics, Hazard and Risk Mitigation, InTech, 2017, https://doi.org/10.5772/66215. https://www.intechopen.com/books/earthquakes-tectonics-hazard-and-risk-mitigation.
[10] EPRI, A Criterion for Determining Exceedance of the Operating Basis Earthquake, Jack R. Benjamin and Associates Inc, 1988. NP - 5930.
[11] D.J. Wald, V. Quitoriano, T.H. Heaton, Relationships between peak ground acceleration, peak ground velocity, and modified Mercalli intensity in California, Earthquake Spectra 15 (3) (August 1999) 557–564.
[12] U. S. Nuclear Regulatory Commission, Development of Floor Design Response Spectra for Seismic Design of Floor-supported Equipment or Components, USNRC, February, 1978. Regulatory Guide 1.122, Revision 1.
[13] EPRI, Guidelines for Nuclear Plant Response to an Earthquake, EPRI NP-6695, MPR Associated, Inc, December, 1989. Final Report.
[14] H.W. Jang, J.-W. Jung, J.-W. Hong, Fatigue fracture analysis of curved pipes under cyclic loading, J. Comput. Struct. Eng. Inst. Korea 29 (4) (August, 2016) 363–368, https://doi.org/10.7734/COSEIK.2016.29.4.363.
[15] C. Seyong, P. Sooyong, C. Sanghyun, Residual life assessment of a concrete floating pier, J. Korean Soc. Hazard. Mitig. 16 (5) (October, 2016) 31–39, https://doi.org/10.9798/KOSHAM.2016.16.5.31.
[16] http://strongmotioncenter.org/vdc/scripts/download_tar.plx [Accessed 07 2017].
[17] KEPCO and KHNP, APR1400 Design Control Document Tier 2, KHNP Nuclear Power Education Institute (NPEI), December, 2014 [Online], https://www.nrc.gov/docs/ML1500/ML15006A042.pdf [April 16 2017].
[18] EPRI, Guidelines for Nuclear Power Plant Response to an Earthquake, Electric Power Research Institute, October 2015. Technical Report 3002005284.